

**The behaviour of parent and daughter nuclides in aerosols released in radiological dispersion events
a study of a SrTiO₃ source**

van Maris, V. R.; Naji, M.; Di Lemma, F.G.; Colle, J-Y; Bykov, D.; Konings, R. J M

DOI

[10.1002/jrs.5076](https://doi.org/10.1002/jrs.5076)

Publication date

2017

Document Version

Final published version

Published in

Journal of Raman Spectroscopy

Citation (APA)

van Maris, V. R., Naji, M., Di Lemma, F. G., Colle, J.-Y., Bykov, D., & Konings, R. J. M. (2017). The behaviour of parent and daughter nuclides in aerosols released in radiological dispersion events: a study of a SrTiO₃ source. *Journal of Raman Spectroscopy*, 48(4), 549-559. <https://doi.org/10.1002/jrs.5076>

Important note

To cite this publication, please use the final published version (if applicable).
Please check the document version above.

Copyright

Other than for strictly personal use, it is not permitted to download, forward or distribute the text or part of it, without the consent of the author(s) and/or copyright holder(s), unless the work is under an open content license such as Creative Commons.

Takedown policy

Please contact us and provide details if you believe this document breaches copyrights.
We will remove access to the work immediately and investigate your claim.

The behaviour of parent and daughter nuclides in aerosols released in radiological dispersion events: a study of a SrTiO₃ source

V. R. van Maris,^{a,b} M. Naji,^b F. G. Di Lemma,^{a,b} J.-Y. Colle,^{b*} D. Bykov^a and R. J. M. Konings^{a,b}



During rapid high-temperature events, like a terrorist attack with radiological dispersal device, radiological material will be released into the environment. In these scenarios, the ratio between parent and daughter nuclides can be used for nuclear forensic investigations to determine the age of the used radioactive source. We have used fast laser heating to produce aerosols of a material often found in radioisotope thermoelectric generators. To investigate the behaviour of SrTiO₃, we have recreated pure and mixed samples, mimicking several parent-to-daughter ratios. By combining scanning electron microscopy and energy-dispersive X-ray spectroscopy analysis with Raman spectroscopy, we were able to distinguish different elements and phases present in the aerosols. Two types of aerosols have been identified: individual aerosols from a few micrometre to a few tens of micrometre and agglomerates of smaller aerosols from a few hundred nanometre to a few micrometre. The bigger aerosols, formed from mechanically expelled liquefied material, showed a parent-to-daughter ratio that stays close to the value that would be anticipated by the initial composition of the material, but in the agglomerates, formed from vaporised material, the presence of the daughter elements reduces significantly due to differences in the condensation behaviour. © 2017 The Authors. *Journal of Raman Spectroscopy* Published by John Wiley & Sons Ltd.

Additional Supporting Information may be found online in the supporting information tab for this article.

Keywords: radiological dispersal device; Raman spectroscopy; aerosol characterisation; nuclear forensics; strontium titanate

Introduction

Radioactive sources can be misused to create a radiological dispersal device (RDD) (a.k.a. 'dirty bomb'). The source material is dispersed during a rapid high-temperature event with a considerable possibility that radiological material will be released into the environment. A likely material that could be used for this is Strontium-90 (⁹⁰Sr), which was used in the form of SrTiO₃ as a fuel for radioisotope thermoelectric generators (RTGs) that use the heat of radioactive decay to generate electricity. In the past, RTGs were used at remote monitoring sites and unmanned lighthouses and are currently still being used in space applications. Some of these terrestrial RTGs have not been decommissioned yet, and those located at unmanned sites are vulnerable for theft and misuse, because they are guarded with limited security measures.^[1]

Radioactive materials can damage human tissue through external radiation or internal radiation upon inhalation or ingestion. The risk of inhaling radioactive particles related to such a detonation depends on the aerodynamic equivalent diameter (AED) of the aerosols. Particles that can be inhaled are required to have an AED < 10 μm, and those that are smaller than AED < 0.1 μm will even be likely to be absorbed into the bloodstream upon inhalation.^[2] Additionally, recent studies^[3] show that also the crystalline form influences the cytotoxicity. For instance, in the case of TiO₂, rutile nanoparticles induce toxic effects, while anatase nanoparticles do not.

Many studies were performed to understand the consequences of radiological dispersion events (RDEs). Different computational models have been used to study dispersion effects. However, because the smallest motions in the atmosphere are hard to pre-

dict but still influence the outcome, results from these models are always a compromise between completeness and time frames.^[4,5]

Explosion experiments have been conducted to research aerosol types and sizes.^[6,7] The results are used to determine the extend of the exclusion zone that should be evacuated in case of a RDD detonation and to determine the perimeters that have to be decontaminated before daily life can be resumed.^[8,9] Various authors^[7,10] report that two different aerosol morphologies are created in these events, which are the result of different formation processes. It is suggested that the larger spherical particles, with an AED of a few micrometre, originate from the liquefied material and are expelled by the mechanical shock.^[10] Smaller particles, with an AED between ten to a few hundred nanometre,

* Correspondence to: Jean-Yves Colle, European Commission, Joint Research Centre (JRC), Directorate for Nuclear Safety and Security, Nuclear Fuel Safety Unit, Postfach 2340, 76125 Karlsruhe, Germany.
Email: Jean-Yves.Colle@ec.europa.eu

This is an open access article under the terms of the Creative Commons Attribution-NonCommercial-NoDerivs License, which permits use and distribution in any medium, provided the original work is properly cited, the use is non-commercial and no modifications or adaptations are made

a Delft University of Technology, Faculty of Applied Physics, Department of Radiation Science and Technology, Nuclear Energy and Radiation Applications Section, Mekelweg 15, 2629 JB Delft, The Netherlands

b European Commission, Joint Research Centre (JRC), Directorate for Nuclear Safety and Security, Nuclear Fuel Safety Unit, Postfach 2340, 76125 Karlsruhe, Germany

are formed by rapid condensation of the vapour and are generally observed as agglomerates.

When time passes, the radioactive inventory of the source changes, strontium-90 ($^{90}_{38}\text{Sr}$) decays into yttrium-90 ($^{90}_{39}\text{Y}$) and subsequently into zirconium-90 ($^{90}_{40}\text{Zr}$). Because the half-life of $^{90}_{38}\text{Sr}$ and $^{90}_{39}\text{Y}$ is known,^[11] the amount of each material can be calculated for any time after the production of the source and, therefore, also the ratio between parent and daughter nuclides. In nuclear forensics, this ratio is often used to determine the date of production.

The current research is, in particular, intended to find out whether the ratio between parent and daughter nuclides of the radioactive source materials remains unchanged in aerosols formed after the rapid high-temperature event. For instance, one can imagine that the elements behave differently and the partition over different aerosol size affects the ratio between parent and daughter nuclides. To do so, we have produced aerosols from recreated pure and mixed samples to mimic the parent to daughter ratios. The combination of multiple techniques, mainly scanning electron microscopy (SEM), energy-dispersive X-ray spectroscopy (EDX) and Raman spectroscopy enable us to gain information on the aerosols size, composition and stable phase formed during such an event.

Materials and methods

The radiological dispersion events setup

To create the aerosols in a rapid high-temperature event, similar to those of a RDD, the radiological dispersion events setup (RADES) has been used. The RADES has been described extensively and is capable of rapidly increasing the temperature of a small sample by means of a laser pulse.^[12] Contrary to those experiments, where the laser power is controlled by a PID controller, in these experiments, the laser power is set at a fixed value and turned on for a predefined period of time.

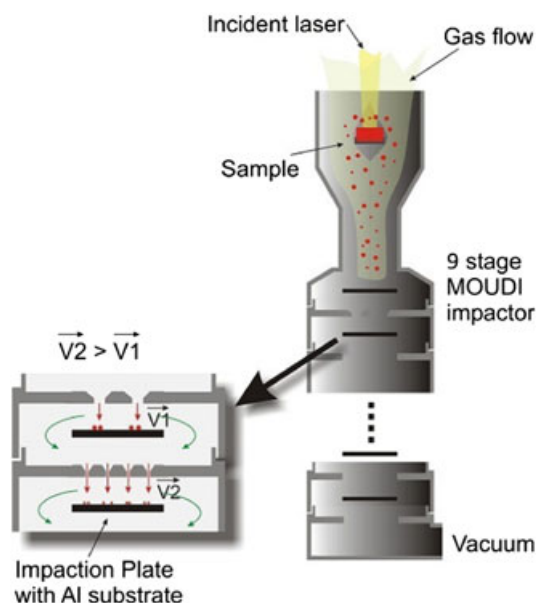


Figure 1. A scheme of the inside of the micro-orifice uniform deposit impactor (MOUDI).^[10] [Colour figure can be viewed at wileyonlinelibrary.com]

Table 1. Nominal cutoff sizes for each stage.^[10]

Stage	Nominal cutoff size μm
0	18
1	10
2	5.6
3	3.2
4	1.8
5	1.0
6	0.56
7	0.32
8	0.18

The aerosol collection system is a MSP Micro-Orifice Uniform Deposit Impactor (MOUDI) model 110R-MRD371, which consists in this setup of nine impactor plates (numbered from 0 to 8) on which the aerosols are collected (Fig. 1). These stages are designed in such a way that when an airflow of 30 L/min is maintained, the probability that a particle with an AED of the nominal cutoff size will impact on this plate exceeds 50%. The nominal cutoff size for each stage is given in Table 1. More information on how this MOUDI works can be found in the reference.^[13]

Samples

Although it is intended to describe the behaviour of radioactive elements, for simplicity reasons, we decided to use the stable isotopes of the relevant elements, as the isotopic composition will not influence the chemical behaviour.

The decay of $^{90}_{38}\text{Sr}$ occurs with a half-life of $T_{1/2} = 28.64$ years, while the half-life of $^{90}_{39}\text{Y}$ is much shorter: $T_{1/2} = 64.1$ h.^[11] So depending on the production date, the source will contain only small amounts of $^{90}_{39}\text{Y}$ that decays to the stable $^{90}_{40}\text{Zr}$. Both decays occur through beta emission. Very little structural damage is produced by the beta decay.^[14] The recoil energy of the $^{90}_{38}\text{Sr}$ and of the $^{90}_{39}\text{Y}$ atoms is lower than the threshold displacement energy. Thus, the beta decay of $^{90}_{38}\text{Sr}$ into $^{90}_{40}\text{Zr}$ is unable to generate defects.

At room temperature, SrTiO_3 has a perovskite cubic structure (space group $Pm\bar{3}m$) where Sr, Ti and O occupy respectively the 1a, 1b and 3c sites. Upon $^{90}_{38}\text{Sr}$ nuclear decay, $^{90}_{39}\text{Y}$ and $^{90}_{40}\text{Zr}$ are supposed to occupy the same cationic site (1a). It is shown that cubic perovskite SrTiO_3 can accommodate only up to 8 mol% of Y in the 1a site.^[15] For higher Y concentrations, a two-phase mixture was obtained with mainly SrTiO_3 and $\text{Y}_2\text{Ti}_2\text{O}_7$. Similarly, it is shown that cubic perovskite zirconium titanite is unstable, and it optimises its geometry by changing into the orthorhombic scrutinyite structure.^[14]

In order to investigate the behaviour of these materials, we have performed our experiments on four sets of compounds grouped in Table 2.

Pure titanates

The first group contains the 'pure titanate' compounds. Experiments were performed with SrTiO_3 , $\text{Y}_2\text{Ti}_2\text{O}_7$ and ZrTiO_4 separately, in order to achieve a deep understanding of their individual behaviour. SrTiO_3 and $\text{Y}_2\text{Ti}_2\text{O}_7$ were obtained by mixing stoichiometric amounts of SrCO_3 , Y_2O_3 and TiO_2 anatase reagents of high purity in a Retsch Mixer Mill MM400. The materials were mixed for at least 6 h in a stainless steel jar with a zirconium inner coating and a zirconium ball in the vibrational mill. Afterwards, the powders were pressed into pellets at a pressure of 7 tonnes or

Table 2. Details of the samples that were used in this research

Sample name	Sample composition	Origin	Known impurities
S1	SrTiO ₃	synthesised	< 10%(ZrO ₂)
Y1	Y ₂ Ti ₂ O ₇	synthesised	< 5%(TiO ₂)
Z1	ZrTiO ₄	commercial	< 1 %
SY1	(Sr _{0.99} Y _{0.01})TiO ₃	synthesised	< 1 %
SY2	(Sr _{0.98} Y _{0.02})TiO ₃	synthesised	< 1 %
SY4	(Sr _{0.96} Y _{0.04})TiO ₃	synthesised	< 1 %
SY8	(Sr _{0.92} Y _{0.08})TiO ₃	synthesised	< 5 % (Y ₂ Ti ₂ O ₇)
SY50	50% SrTiO ₃ + 50% Y ₂ Ti ₂ O ₇	mixed	
SZ50	50% SrTiO ₃ + 50%ZrTiO ₄	mixed	
YZ50	50% Y ₂ Ti ₂ O ₇ + 50%ZrTiO ₄	mixed	
SYZ1	40% (Sr _{0.99} Y _{0.01})TiO ₃ + 60%ZrTiO ₄	mixed	
SYZ2	54% (Sr _{0.99} Y _{0.01})TiO ₃ + 46%ZrTiO ₄	mixed	

All samples contain titanium and oxide. The sample names containing the letter 'S' contain strontium, 'Y' contain yttrium and 'Z' contain zirconium. The number in the second group indicates the percentage of yttrium in the sample. The number 50 in the third group indicates that these samples are a 50% mixture, and the numbers in the first and fourth group indicate different samples.

68.5 kN for approximately 5 min. Heat treatment was applied for at least 15 h in a Borel Special Furnace TL 1100-8 at 1000°C. This procedure has already been described previously.^[16] ZrTiO₄ was obtained commercially.

Yttrium-doped strontium titanates

The second group contains (Sr_{1-x}Y_x)TiO₃ with $x = 0.01, 0.02, 0.04$ and 0.08 , the 'yttrium-doped strontium titanate' compounds. These compounds were synthesised by the same process as the 'pure titanate' compounds. Sample SY1, which is mentioned in Table 2, was only used as a reagent for later samples; no aerosols were produced from this material.

Binary mixtures

Further experiments were done with the three combinations of 50% of the 'pure titanate' compounds to determine if there are any phenomena of interaction between those elements; these are given in the third group containing 'binary' compounds.

Ternary mixtures

Because it is reported that strontium was mainly used in RTGs,^[1] which were in mass production between 1976 and 1990, two samples were made that would represent an age of 38 and 24 years old; these can be found in the fourth group: the 'ternary' mixtures. Attempts to obtain a single phase of compounds described in the groups with binary and ternary mixtures have failed. Therefore, stoichiometric amounts of SrTiO₃, Y₂Ti₂O₇, ZrTiO₄ and (Sr_{1-x}Y_x)TiO₃ in powder form were intimately mixed to get a good homogeneity and pressed with an hydraulic press into pellets of 5 mm in diameter and a few millimetres in height. No further heat treatment was performed. An overview of the investigated samples is presented in Table 2.

Analytical equipment

X-Ray Diffraction

X-Ray Diffraction (XRD) measurements were performed using a PANalytical X'Pert Pro diffractometer with Cu-K α radiation. The patterns were scanned through steps of 0.008 2- θ° , between 10

and 80 2- θ° , with a total measuring time per sample of 40 min. Purity of the samples was checked by phase analysis with the HighScore program by implemented matching procedure.

Scanning electron microscopy and energy-dispersive X-ray spectroscopy

After the aerosols are created by the laser pulse and collected by the impactor plates on aluminium sheets, a small piece of approximately 12 mm in diameter was cut from each sheet and examined by SEM and Raman spectroscopy. SEM images, both secondary electron as well as backscatter electron, have been made using a Philips XL 40 SEM. This machine is also used to perform EDX analysis; the elemental compositions are obtained by averaging EDX measurements for each stage.

Raman spectroscopy

Raman analysis of the aerosols deposited on the aluminium sheets was performed using a Horiba Jobin Yvon T64000 spectrometer in the simple monochromator mode. The aerosols were irradiated using an Ar⁺ coherent continuous wave laser emitting at 514.5 nm and x50 long-focal distance objective. The power impinging the sample surface was below 3 mW. The scattered light was filtered using a 514.5-nm edge filter, dispersed using a 1800-gr/mm diffraction grating and focussed on a LN₂-cooled CCD detector. The laser spot size is around 2 μm^2 .

Sample characteristics after synthesis

X-Ray Diffraction

The XRD pattern of sample Y1 (Y₂Ti₂O₇) shows some extra peaks attributed to the TiO₂ phase (< 5% as mentioned in Table 2). All the yttrium-doped strontium titanate samples shows the same features as the pure cubic SrTiO₃. For the composition with 8% Y (sample SY8), extra peaks attributed to Y₂Ti₂O₇ were identified.

Raman spectroscopy

The Raman spectra of the samples after the synthesis, but before the rapid high-temperature event, are shown together with the spectra of the aerosols that are created in the rapid high-temperature event (See Section on Phase Identification of Aerosols: Raman Spectroscopy). In order to compare these spectra amongst themselves, the spectra of the initial materials are also shown, sorted by the four groups (as defined in Table 2), in Fig. S1 to S4.

Pure titanate group

At ambient temperature and pressure, SrTiO₃ has a centro-symmetric space group. The five atoms in the primitive unit cell are located around an inversion centre. At the Brillouin zone centre, the 15 degrees of freedom lead to

$$\Gamma = F_{1u}(\text{acoustic}) + 3 \cdot F_{1u}(\text{optic}) + F_{2u}(\text{optic}) \quad (1)$$

Because all the zone-centre optical modes are of odd parity, no first-order Raman scattering is expected to occur. However in Fig. S1 (Supporting Information), broad peaks are seen between 240 and 420 cm⁻¹ and between 605 and 730 cm⁻¹ involving the combination of two phonons (a second-order Raman process).^[17,18]

Y₂Ti₂O₇ has a cubic pyrochlore structure with a *Fd3m* space group. Factor group analysis for this compound suggests six Raman active modes (*A*_{1g}, *E*_g and *F*_{2g}) and seven infrared active modes (*F*_{1u}):

$$\Gamma = 7 \cdot F_{1u} + A_{1g} + E_g + 4 \cdot F_{2g} \quad (2)$$

The wavenumbers of these vibrational modes in the Y₂Ti₂O₇ sample are in very good agreement with the literature.^[19] The spectrum (Fig. S1 (Supporting Information)) exhibits four characteristic peaks at 304 (*F*_{2g}), 445 (*F*_{2g}), 520 (*A*_{1g}) and 607 cm⁻¹ (*F*_{2g}).

ZrTiO₄ has an orthorhombic α-PbO₂ structure with *Pbcn* space group. The normal vibration modes, as obtained by factor group analysis, suggest 18 Raman-active non-degenerate modes that can be written using the following irreducible representations:

$$\Gamma = 4 \cdot A_g + 5 \cdot B_{1g} + 4 \cdot B_{2g} + 5 \cdot B_{3g} \quad (3)$$

The main Raman peaks are observed at 160, 256, 408, 641 and 800 cm⁻¹ (Fig. S1 (Supporting Information)). The wavenumbers of

these vibrational modes are in very good agreement with those reported in literature.^[20] Except for the mode at 800cm⁻¹ that was assigned to *A*_g symmetry,^[21] a complete assignment of these modes is still unknown.

Yttrium-doped strontium titanate group

Raman spectra of the solid solutions ((Sr_{1-x}Y_x)TiO₃ with *x* = 0.02, 0.04 and 0.08) shows the same Raman features as SrTiO₃, with an interesting behaviour of the broad bands (Fig. S2 (Supporting Information)). These bands generally tend to narrow and slightly down shift when increasing the Y content, most likely because of the expansion of the lattice and the decrease of the static disorder. However, neither extra peaks of TiO₂ nor of Y₂Ti₂O₇ were observed in the Raman spectra of Y1 (Fig. S1 (Supporting Information)) and SY8 (Fig. S2 (Supporting Information)), respectively. It is very likely that the Raman cross section of the Ti-O and Y-O vibration in these compounds is very low compared with SrTiO₃ and (Sr_{1-x}Y_x)TiO₃.

Binary group

The 50% mixed samples (Fig. S3 (Supporting Information)) show mixed Raman features of the individual 'pure titanate' materials. Peaks at 304 and at 520 cm⁻¹ are obviously assigned to Y₂Ti₂O₇ compound, while those at 605 and 730 cm⁻¹ correspond to SrTiO₃.

Ternary group

Finally, samples SYZ1 and SYZ2 with all three elements (Fig. S4 (Supporting Information)) resemble ZrTiO₄ the most. The dominance of the ZrTiO₄ Raman features in the mixed compounds SYZ1 and SYZ2 is mainly due to the high Raman cross section of this material.

Overall, it can be concluded that the synthesised samples reveal limited amounts of impurity according to XRD analysis and the Raman spectra obtained shows great resemblance with spectra found in literature. The synthesis process can be considered to be performed successfully.

Results

Morphology of aerosols: SEM images

Previous observations describe two types of aerosol morphologies created in RDE, which are a result of different processes.^[6,7,10] The larger spherical particles, with an AED of a few micrometre

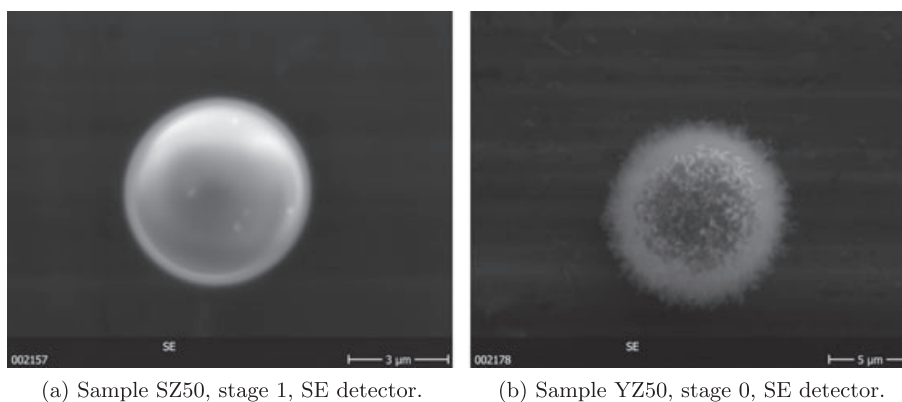
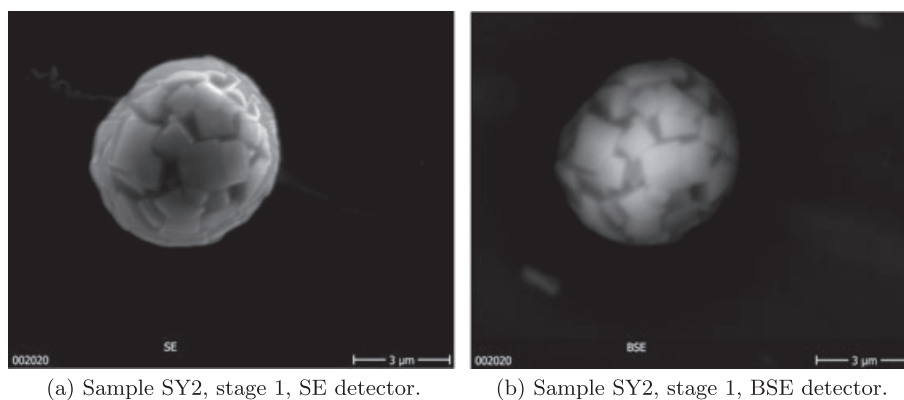


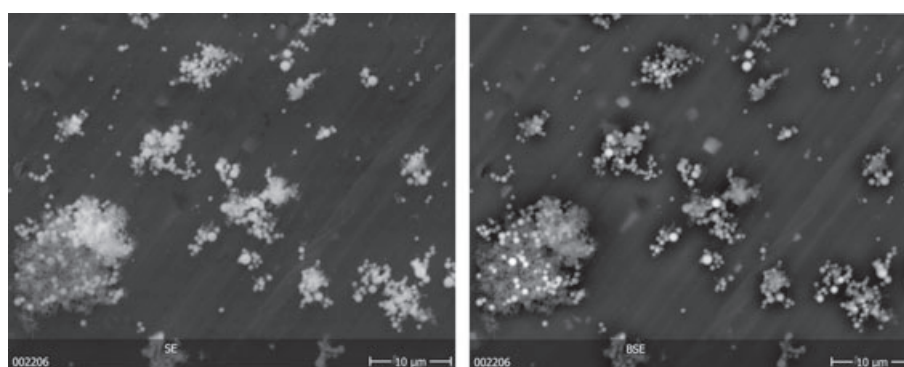
Figure 2. Scanning electron microscopy images: large individual particles can be found on the upper stages, stages where aerosols with a bigger aerodynamic equivalent diameter are found. (a) Sample SZ50, stage 1, secondary electron (SE) detector. (b) Sample YZ50, stage 0, SE detector.



(a) Sample SY2, stage 1, SE detector.

(b) Sample SY2, stage 1, BSE detector.

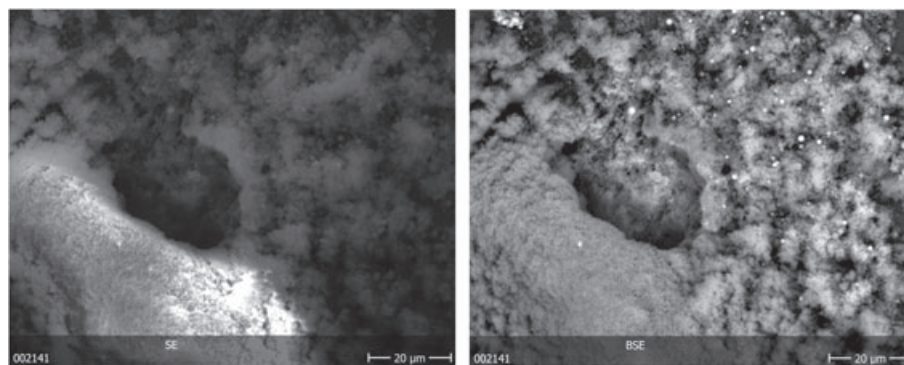
Figure 3. Scanning electron microscopy images: cubical crystallization in large individual particles. (a) Sample SY2, stage 1, secondary electron (SE) detector. (b) Sample SY2, stage 1, backscatter electron detector.



(a) Sample SYZ2, stage 5, SE detector.

(b) Sample SYZ2, stage 5, BSE detector.

Figure 4. Scanning electron microscopy images: small particles that form small agglomerates. (a) Sample SYZ2, stage 5, secondary electron (SE) detector. (b) Sample SYZ2, stage 5, backscatter electron detector.



(a) Sample SZ50, stage 7, SE detector.

(b) Sample SZ50, stage 7, BSE detector.

Figure 5. Scanning electron microscopy images: small particles that form one big agglomerates, showing similarity with a hill made out of grains of sand. (a) Sample SZ50, stage 7, secondary electron (SE) detector. (b) Sample SZ50, stage 7, backscatter electron detector.

(Fig 2), originate from the liquefied material and are expelled by the mechanical shock. The acquired SEM images of the aerosols in this experiment show similar morphologies as the aerosols in the SrTiO₃ experiments conducted earlier.^[10]

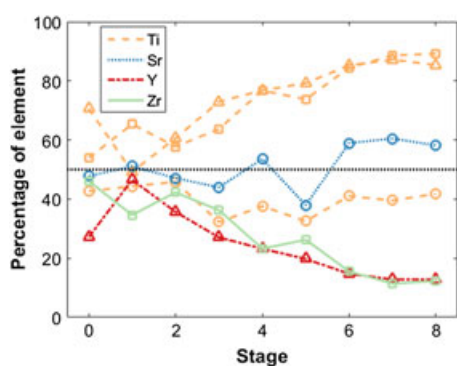
Some of the individual aerosols revealed a crystalline substructure different from the majority of the aerosols; an example is given in Fig. 3. It shows crystallization within the aerosol, where the crystals seem to be cubic and randomly orientated in the

aerosol. This crystallization in the aerosols was only found in samples in stage 1, which suggest a relation to the crystallization from the liquid phase.

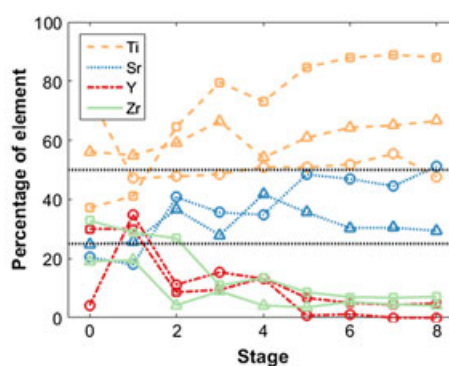
Smaller particles, with an AED between ten to a few hundred nanometre, are formed by the rapid condensation of the vapour and are generally observed as agglomerates (Figs 4 and 5). Table 3 gives an overview of the distribution of individual particles ('I') and agglomerates ('A').

Table 3. An overview of the stages of the different materials with the indication if individual particles ('I') and/or agglomerates ('A') are recognised on the scanning electron microscopy images.

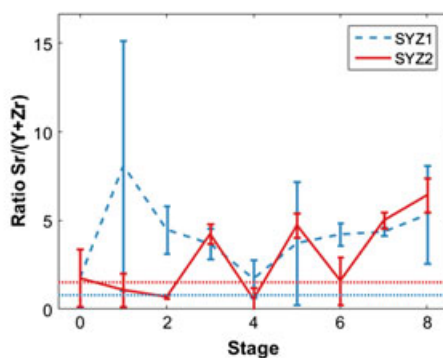
Stage	S1	Y1	Z1	SY2	SY4	SY8	SY50	SZ50	YZ50	SYZ1	SYZ2
0	I	I	I	I	I	I	I	I	I	I	I
1	I	I	I	I	I	I	I	I	I	I	I
2	I	I	I	I	I	I	I	I	I	I	I
3	I	I	I	I	I	I	I	I	I	I	I
4	I+A	I+A	I	I	I	I+A	I	I	I+A	I	I+A
5	I+A	I+A	I+A	I	I+A						
6	A	I+A	I+A	I+A	I+A	I+A	I+A	I+A	I+A	I+A	A
7	A	A	A	A	A	I+A	I+A	A	A	A	A
8	A	A	A	A	A	A	I+A	A	A	A	A



(a) Sample S1 is marked with \circ , sample Y1 is marked with \triangle and sample Z1 is marked with \square . Dotted line indicates expected value for all elements at 50%.



(b) Sample SY50 is marked with \circ , sample SZ50 is marked with \triangle and sample YZ50 is marked with \square . Upper dotted line indicates expected value for Ti at 50%. Lower dotted line indicates expected value for Sr, Y and Zr at 25%.



(c) Ratio between parent and daughter nuclides. Dotted lines indicate expected ratios, 0.7956 for SYZ1 and 1.5189 for SYZ2.

Figure 6. Energy-dispersive X-ray data. The dotted lines indicate the expected values. (a) Sample S1 is marked with \circ , sample Y1 is marked with \triangle and sample Z1 is marked with \square . Dotted line indicates expected value for all elements at 50%. (b) Sample SY50 is marked with \circ , sample SZ50 is marked with \triangle and sample YZ50 is marked with \square . Dotted line indicates expected value for all elements at 50%. (c) Ratio between parent and daughter nuclides. Dotted lines indicate expected ratios, 0.7956 for SYZ1 and 1.5189 for SYZ2. [Colour figure can be viewed at wileyonlinelibrary.com]

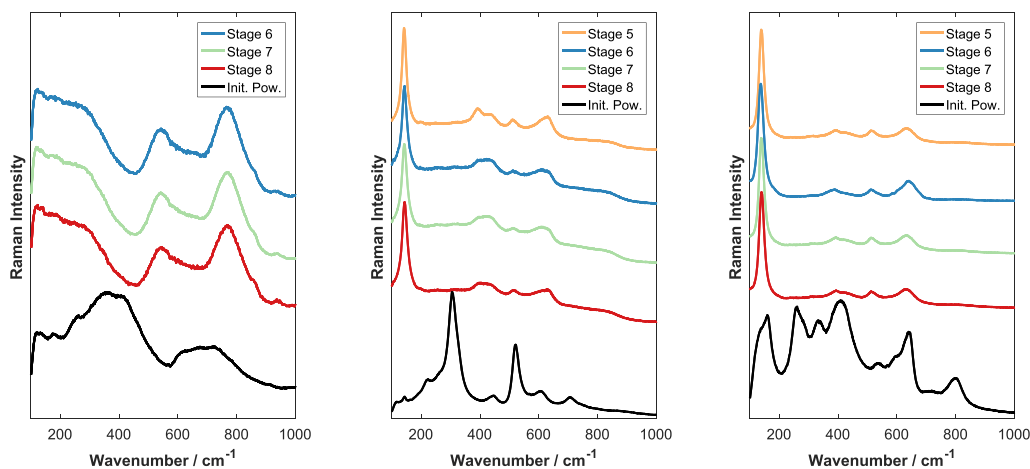
Elementary composition of aerosols: EDX analysis

As described in Section on Scanning Electron Microscopy and Energy-Dispersive X-ray Spectroscopy, EDX analysis was performed to analyse the elemental composition as a function of the particle size of the aerosols and thus identify if partitioning of the parent and daughter nuclides occurs. Some stages contained only few aerosols; therefore, the localisation of the aerosols on the impactor plates was a time-consuming process, and especially for the upper stages, it was sometimes difficult just to find a single aerosol. For that reason, for some stages, the EDX measurements could have only been done at few positions. This results in fluctuating average values and large standard deviations for some of

the stages. Nevertheless, a clear trend has been found in the EDX results, which is presented in Fig. 6.

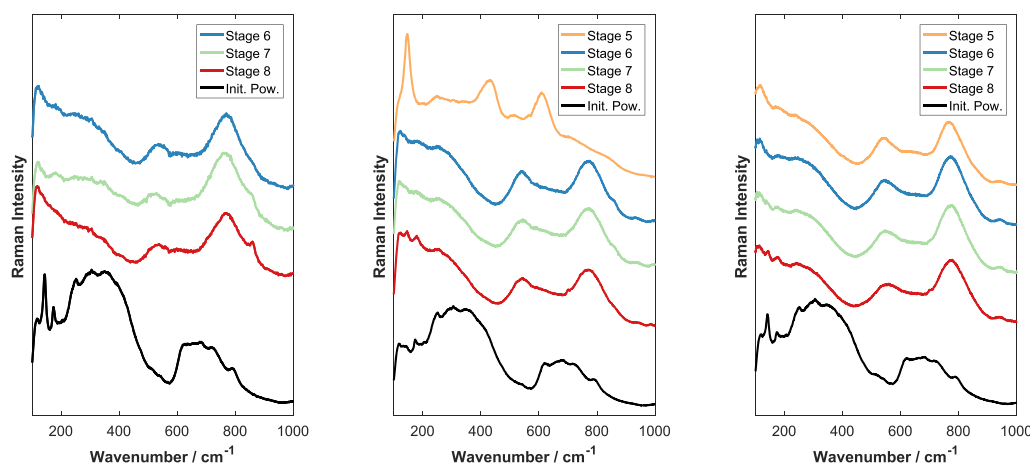
Pure titanate group

Figure 6(a) shows the elemental composition of SrTiO₃, Y₂Ti₂O₇ and ZrTiO₄. For SrTiO₃ (sample S1) the percentage of Sr and Ti stays more or less in the range of the expected value (50% for all samples), but for Y₂Ti₂O₇ (sample Y1) and for ZrTiO₄ (sample Z1) the percentage of Y or Zr decreases and the percentage of Ti becomes higher when the particles become smaller.



(a) Aerosols on different stages and the initial powder (Init. Pow.) before aerosol creation, of sample S1. (b) Aerosols on different stages and the initial powder (Init. Pow.) before aerosol creation, of sample Y1. (c) Aerosols on different stages and the initial powder (Init. Pow.) before aerosol creation, of sample Z1.

Figure 7. Raman spectra of aerosols (part 1). Aerosols on different stages and the initial powder (Init. Pow.) before aerosol creation of samples (a) S1, (b) Y1 and (c) Z1. [Colour figure can be viewed at wileyonlinelibrary.com]



(a) Aerosols on different stages and the initial powder (Init. Pow.) before aerosol creation, of sample SY2. (b) Aerosols on different stages and the initial powder (Init. Pow.) before aerosol creation, of sample SY4. (c) Aerosols on different stages and the initial powder (Init. Pow.) before aerosol creation, of sample SY8.

Figure 8. Raman spectra of aerosols (part 2). Aerosols on different stages and the initial powder (Init. Pow.) before aerosol creation of samples (a) SY2, (b) SY4 and (c) SY8. [Colour figure can be viewed at wileyonlinelibrary.com]

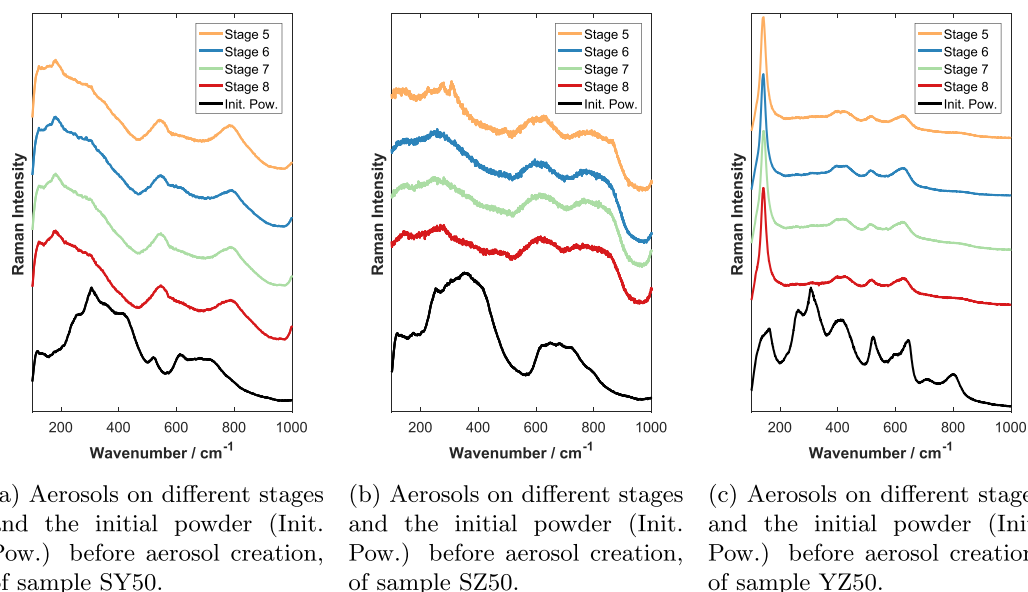
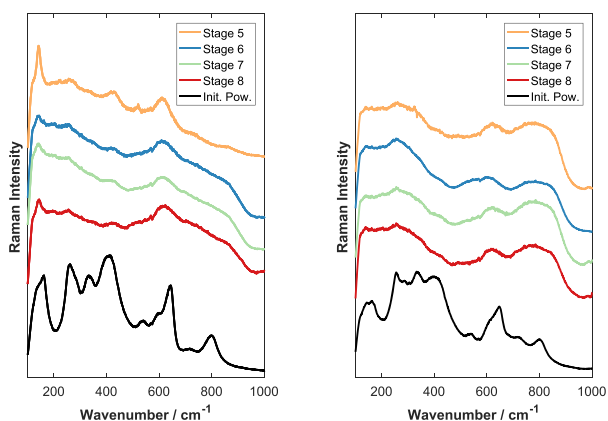


Figure 9. Raman spectra of aerosols (part 3). Aerosols on different stages and the initial powder (Init. Pow.) before aerosol creation of samples (a) SY50, (b) SZ50 and (c) YZ50. [Colour figure can be viewed at wileyonlinelibrary.com]



(a) Aerosols on different stages and the initial powder (Init. Pow.) before aerosol creation, of sample SYZ1. (b) Aerosols on different stages and the initial powder (Init. Pow.) before aerosol creation, of sample SYZ2.

Figure 10. Raman spectra of aerosols (part 4). Aerosols on different stages and the initial powder (Init. Pow.) before aerosol creation of samples (a) SYZ1 and (b) SYZ2. [Colour figure can be viewed at wileyonlinelibrary.com]

Binary group

Figure 6(b) shows the EDX data of the 'binary' compounds (sample SY50, SZ50 and YZ50). Here, the same observations can be reported as in the figure of the 'pure titanates'. For sample SY50, it was observed that the titanium content stays fairly constant around the expected value, while the titanium concentration in strontium titanate (sample S1) was lower than the expected value and the titanium concentration in yttrium titanate (sample Y1) was higher than expected. The strontium contents start at the expected value and then increases towards the lower stages, while the yttrium contents show the opposite trend. In sample SZ50, the titanium content is more present in all stages, but this surplus increases towards lower stages. The strontium con-

tent stays close to its expected value, and the zirconium content decreases after the first two stages. In sample YZ50, the titanium content also increases, although to a much higher percentage, because both the yttrium and zirconium contents decrease in the lower stages.

Ternary group

For the samples that have the same elemental content as radioactive samples made in 1976 and 1990, the ratio between parent (Sr) and daughter elements (Y and Zr) is shown in Fig 6(c). The ratio increases towards the lower stages, which means that the determination of the production date using the ratio is not possible for smaller AED.

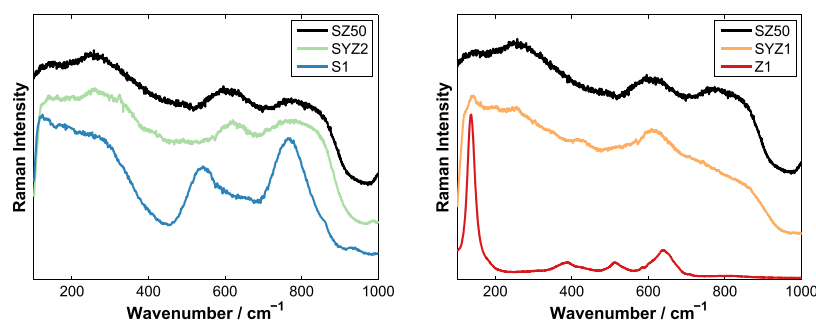
Phase identification of aerosols: Raman spectroscopy

The Raman spectra of the aerosols collected on the stages are presented in Figs 7–10. For comparison, the bottom spectrum in every figure represents the Raman spectrum of the material (in powder form) before the rapid high-temperature event.

Pure titanate group

The Raman spectra of the aerosols produced from SrTiO_3 does not correspond to that of SrTiO_3 before the experiments. There are peaks present around 170, 545 and 790 cm^{-1} , as can be seen in Fig 7(a). The EDX results give no indication for other elements to be present in the aerosols.

By comparing this spectrum to the Raman spectra of SrTiO_3 published in literature,^[17,18,22] it can be seen that these modes correspond to three first-order phonon vibrations observed at approximately 180, 540 and 780 cm^{-1} attributed to TO_2 , TO_4 and LO_4 modes, respectively. As discussed previously, the room temperature Raman spectrum of SrTiO_3 is dominated by second-order Raman scattering. However, Raman scattering of SrTiO_3 has shown that first-order Raman scattering modes can actually be observed when the local symmetry is broken because of various factors, such as strain effects, the presence of impurities or defects and oxygen vacancies.^[23] For nanoparticles of SrTiO_3 ,



(a) Aerosols of sample SZ50, SYZ2 and S1. (b) Aerosols of sample SZ50, SYZ1 and Z1.

Figure 11. Raman spectra comparison with sample SZ50. (a) Aerosols of sample SZ50, SYZ2 and S1. (b) Aerosols of sample SZ50, SYZ1 and Z1. [Colour figure can be viewed at wileyonlinelibrary.com]

the origin of symmetry breaking comes from frozen surface dipoles or from local tetragonal arrangement as well as the presence of nanoscopic polar domains because of the incorporated impurities.^[24] The presence of these modes in the Raman spectra of the aerosols of SrTiO₃ can be due to many factors. Very likely, strain effects, frozen surface dipoles and nanometric domains can be formed when the rapidly heated material comes in contact with the air and forms the aerosols during the RADES experiment.

Although the Raman spectrum of the initial powders of Y₂Ti₂O₇ and ZrTiO₄ are very different from each other (which was determined in Section on Pure Titanate Group), the Raman spectrum of the aerosols show great resemblance when comparing Fig 7(b) and (c). It is evident that the aerosols reveal Raman spectra different from the initial material for both samples, and remarkably, the aerosols of Y₂Ti₂O₇ resemble the aerosols of ZrTiO₄. The peak around 143 cm⁻¹ is a well-known feature in the spectrum of TiO₂. The obtained Raman patterns correspond to the spectrum of a TiO₂ rutile and anatase mixture. Bands around 144 (*E_g*), 197 (*E_g*), 399 (*B_{1g}*), 514 (*A_{1g}*, *B_{1g}*), and 639 cm⁻¹ (*E_g*) are attributed to the anatase phase,^[25] while those at 447 (*E_g*), 612 (*A_{1g}*) and 826 cm⁻¹ (*B_{2g}*) are attributed to the rutile phase.^[26] Presence of both phases in the Raman spectra was well documented in literature,^[27] but the reasons why these different phases are formed is poorly understood. Composition, temperature and the rate of crystallization, may all affect the polymorphology. Here, we suggest that the presence of the rutile phase is very likely due to the rapid quenching of this high-temperature-stable phase. Few studies show that the presence of a suitable doping agent strongly affects the kinetics of this process. Indeed, some metal species can occupy interstitial positions or induce structural changes in metal oxide structures, as is the case of Nb, V, and Ce loaded onto TiO₂.^[28] In accordance with EDX results, it is very likely that the presence of Y or Zr in TiO₂ aerosols affects the kinetic of this process and the freezing of the rutile phase.

Yttrium-doped strontium titanate group

The Raman spectrum of the aerosols obtained from SY2, SY4 and SY8 are comparable with the Raman spectrum of SrTiO₃ (sample S1). It is important to note that we observed a slight change in the shape of the continuous background and the intensity ratio of few bands (especially for the band centred at 520 cm⁻¹ relative to the band at 545 cm⁻¹). This is very likely due to an electronic process during the Raman measurements. The aerosols were measured on aluminium substrate that can enhance the Raman scattering of few modes through a charge transferring process. Although the EDX measurements suggest a higher percentage of Y present in the aerosols, the continuous back-

ground and the large Raman bands do not allow us to observe any feature attributed to components containing Y.

Binary group

Whereas the characterisation of Raman features corresponding to sample SY50 and sample YZ50 spectra is almost straightforward, the Raman features of sample SZ50 needs to be discussed more thoroughly.

The Raman spectra of aerosols of sample SY50 are dominated by features of sample S1 with the presence of a Raman signature of TiO₂ near 145 cm⁻¹ (Fig. 9(a)). The change in intensity of the high wavenumber modes is a result of the change in the shape of the background. Sample YZ50 consists mainly of TiO₂ because it compares well with sample Y1 and Z1 (Fig. 9(c)); according to the EDX measurements, only a minor percentage of the aerosols consists of Zr and Y. The Raman spectra of the aerosols of sample SZ50 finally prove to provide the link between the aerosols of the SrTiO₃ sample and the aerosols of the Y₂Ti₂O₇ and ZrTiO₄ samples. Figure 11(a) and (b) shows sample SZ50 in black, compared with different other samples. In Fig. 11(a), some features can be seen that connect the spectrum of sample SZ50 with the that of SrTiO₃ (sample S1), especially the band around 250 cm⁻¹ and the peak at 770 cm⁻¹ that provide here the resemblance. In Fig. 11(b), it becomes clear that the peak at 610 cm⁻¹ originates from ZrTiO₄. This indicates that the Raman spectra of aerosols of sample SZ50 are dominated by features attributed to both SrTiO₃ and ZrTiO₄.

Ternary group

The two intermediate samples that are shown in Fig. 11(a) and (b) are the samples that mimic the material of a radioactive source that was made in 1976 and 1990. Sample SYZ2 in Fig. 11(a) contains approximately 60.3% Sr, 0.6% Y and 39.1% Zr. Sample SYZ1 in Fig. 11(b) contains approximately 44.3% Sr, 0.5% Y and 55.2% Zr. Their Raman spectra confirm that they fill up the gap between the 'pure' materials and the 50% mixtures. Overall, it seems like almost all the aerosols of the mixed materials show a behaviour that can be explained by comparing them with the 'pure' or synthesised materials.

Discussion

The elemental composition of the aerosols created by the experiments with strontium, yttrium and zirconium titanate deviated from the starting material for the aerosols with a smaller AED. These phenomena were already clearly visible for the aerosols of SrTiO₃, Y₂Ti₂O₇ and ZrTiO₄ separately. Strontium concentrates

in the agglomerates of smaller particles, while yttrium and zirconium are less present in the smaller aerosols. In the samples where strontium and one or more of its daughter nuclides are present, the results show a combination of the behaviour of the individual materials. Because the difference between the elemental ratios and their theoretical value is not proportional to the age of the samples, age determination of the source material is not possible by analysing the ratio in the smaller aerosols produced by phase transition.

With a smaller AED, the experimental data reveal that titanium oxide is present in the aerosols of the samples with significant yttrium or zirconium content. In these particles, a lower percentage of yttrium and zirconium and a higher percentage of titanium are measured by EDX analysis, and also, the Raman spectra reveal titanium oxide. This is considered to be the main reason why the zirconium content in the aerosols of the samples that mimic older materials does not exceed the strontium content: a higher amount of yttrium and zirconium titanate in the material before the RDE results in a higher amount of titanium oxide in the aerosols. Whether this is also the case for the bigger individual particles cannot be determined because the individual particles are too small to perform Raman spectroscopy on.

Another consequence of the fact that titanium oxide was present in the aerosols is that the aerosols in RDD scenarios possess an additional health risk, besides the radiological risk. It is reported that titanium oxide nanoparticles in the rutile crystalline form can cause cytotoxic, neoplastic and genotoxic effects.^[3]

The Raman spectra of the aerosols with strontium titanate also showed first-order Raman scattering. This is an interesting outcome because first-order Raman is symmetrically forbidden in single-crystal strontium titanate. It is therefore suggested that the aerosols contain impurities and have many grain boundaries that allow the first-order Raman scattering to dominate in the spectrum.

Conclusion

The ratio between parent and daughter nuclides is an important parameter in RDD scenarios, because this is used in nuclear forensics to determine the age of the material. We have used fast laser heating to produce aerosols of a material often found in RTGs, SrTiO₃. To investigate the behaviour of SrTiO₃, we have recreated pure and mixed samples mimicking the parent to daughter ratios. In earlier experiments, it was already shown by SEM analysis that two types of aerosols are created. The bigger individual aerosols show a ratio that stays close to the value that would be anticipated by the composition of the initial material used in the RDD and agglomerates of smaller aerosols in which the presence of the daughter nuclides reduces significantly. For these smaller aerosols, age determination of the original material can be ruled out; for the bigger aerosol, stronger experimental evidence with smaller standard deviations is needed to determine their usefulness for this purpose.

List of Acronyms

AED	aerodynamic equivalent diameter
BSE	backscatter electron
TUD	Delft University of Technology
EC	European Commission
EDX	energy-dispersive X-ray spectroscopy

GENTLE Graduate and Executive Nuclear Training and Lifelong Education

ITU Institute for Transuranium Elements

JRC Joint Research Centre

MOUDI Micro-Orifice Uniform Deposit Impactor

RADES radiological dispersion events setup

RDD radiological dispersal device

RDE radiological dispersion event

RTG radioisotope thermoelectric generator

SE secondary electron

SEM scanning electron microscopy

XRD X-ray diffraction

Acknowledgements

This work is part of the Graduate and Executive Nuclear Training and Lifelong Education (GENTLE) Project, supported by the Institute for Transuranium Elements (ITU) of the Joint Research Centre (JRC) of the European Commission (EC), coordinated by the Delft University of Technology (TUD) and executed by V.R. van Maris under the conditions of User Access Agreement no. 228675. V.R. van Maris would further like to underline the pleasant collaboration with the co-authors and acknowledge the contributions made by B. Cremer, O. Dieste-Blanco, M. Ernstberger, K. Goubitz, P. Jagai, D. Manara, K. Mayer, G. Rasmussen, M. Sierig, A. Tacu, T. Wiss and J. Zappey.

References

- [1] C. D. Ferguson, T. Kazi, J. Perera, *Commercial Radioactive Sources: Surveying the Security Risks*, Monterey Institute of International Studies, Monterey, U.S.A., **2003**.
- [2] L. L. N. Guarieiro, A. L. N. Guarieiro, in *Biofuels - Economy, Environment and Sustainability* (Ed: Z. Fang), IN TECH, Rijeka, Croatia, **2013**, pp. 357–386.
- [3] C. Uboldi, P. Urbán, D. Gilliland, E. Bajak, E. Valsami-Jones, J. Ponti, F. Rossi, *Toxicol. In Vitro* **2016**, *31*.
- [4] R. J. Serafin, E. J. Barron, H. B. Bluestein, S. F. Clifford, L. M. Duncan, M. A. LeMone, D. E. Neff, W. E. Odom, G. J. Pfeffer, K. K. Turekian, T. J. Warmer, J. C. Wyngaard, *Tracking and Predicting the Atmospheric Dispersion of Hazardous Material Releases - Implications for Homeland Security*, National Academy of Sciences, Washington, U.S.A., **2006**.
- [5] Y. Rentai, *Nucl. Sci. Technol.* **2011**, *1*, 7.
- [6] D. S. Lee, E. G. Snyder, R. Willis, R. Fischer, D. Gates-Anderson, M. Sutton, B. Viani, J. Drake, J. Mackinney, *J. Hazard. Mater.* **2010**, *176*, 56.
- [7] F. T. Harper, S. V. Musolino, W. B. Wentz, *Health Phys.* **2007**, *93*, 1.
- [8] Z. Prouza, V. Beckova, I. Cespirova, J. Helebrant, J. Hulka, P. Kuca, V. Michalek, P. Rulik, J. Skrkal, J. Hovorka, *Radiat. Prot. Dosim.* **2010**, *139*, 519.
- [9] P. Rulik, Z. Prouza, J. Hovorka, V. Beckova, I. Cespirova, A. Fronka, J. Helebrant, J. Hulka, P. Kuca, J. Skrkal, *Radiat. Prot. Dosim.* **2013**, *154*, 207.
- [10] F. G. Di Lemma, *Characterisation of aerosols from simulated Radiological Dispersion Events*. Ph.D. Thesis, Delft University of Technology, **2015**.
- [11] J. Magill, G. Pfenning, J. Galy, *Karlsruher Nuklidkarte*, European Communities, Karlsruhe, Germany, **2006**.
- [12] F. G. Di Lemma, J. Y. Colle, M. Ernstberger, G. Rasmussen, H. Thiele, R. J. M. Konings, *J. Aerosol Sci.* **2014**, *70*, 36.
- [13] V. A. Marple, K. L. Rubow, S. M. Behm, *Aerosol Sci. Technol.* **1991**, *14*, 434.
- [14] N. A. Marks, D. J. Carter, M. Sassi, A. L. Rohl, K. E. Sickafus, B. P. Uberuaga, C. R. Stanek, *J. Phys.: Condens. Matter* **2013**, *25*, 065504.
- [15] S. Hui, A. Petric, *J. Electrochem. Soc.* **2002**, *149*, J1.
- [16] X. Huang, H. Zhao, W. Shen, W. Qiu, W. Wu, *J. Phys. Chem. Solids* **2006**, *67*, 2609.
- [17] W. G. Nilsen, J. G. Skinner, *J. Chem. Phys.* **1968**, *48*, 2240.
- [18] A. Tkach, T. M. Correia, A. Almeida, J. Agostinho Moreira, M. R. Chaves, O. Okhay, P. M. Vilarinho, I. Gregora, J. Petzelt, *Acta Mater.* **2011**, *59*, 5388.

- [19] N. Sellami, G. Sattonnay, C. Grygiel, I. Monnet, A. Debelle, C. Legros, D. Menut, S. Miro, P. Simon, J. L. Bechade, L. Thomé, *Nucl. Instrum. Methods Phys. Res., Sect. B* **2015**, 365, 371.
- [20] Y. K. Kim, H. M. Jang, *J. Appl. Phys. (Melville, NY, U. S.)* **2001**, 89, 6349.
- [21] Y. K. Kim, H. M. Jang, *Solid State Commun.* **2003**, 127, 433.
- [22] Y. L. Du, G. Chen, M. S. Zhang, *Solid State Commun.* **2004**, 130, 577.
- [23] F. A. Rabuffetti, H. S. Kim, J. A. Enterkin, Y. Wang, C. H. Lanier, L. D. Marks, K. R. Poeppelmeier, P. C. Stair, *Chem. Mater.* **2008**, 20, 5628.
- [24] J. Petzelt, T. Ostapchuk, I. Gregora, M. Savinov, D. Chvostova, J. Liu, Z. Shen, *J. Eur. Ceram. Soc.* **2006**, 26, 2855.
- [25] T. Ohsaka, F. Izumi, Y. Fujiki, *J. Raman Spectrosc.* **1978**, 7, 321.
- [26] V. Swamy, B. C. Muddle, Q. Dai, *Appl. Phys. Lett.* **2006**, 89, 163118.
- [27] H. Yin, Y. Wada, T. Kitamura, S. Kambe, S. Murasawa, H. Mori, T. Sakata, S. Yanagida, *J. Mater. Chem.* **2001**, 11, 1694.
- [28] E. Uyanga, A. Gibaud, P. Daniel, D. Sangaa, G. Sevjidsuren, P. Altantsog, T. Beuvier, C. H. Lee, A. M. Balagurov, *Mater. Res. Bull.* **2014**, 60, 222.

Supporting information

Additional Supporting Information may be found online in the supporting information tab for this article.